

Autorização concedida ao Repositório Institucional da Universidade de Brasília (RIUnB) pelo Prof. Dr. Antonio Carlos de Oliveira Miranda, em 28 de setembro de 2018, para disponibilizar o trabalho, gratuitamente, para fins de leitura, impressão e/ou download, a título de divulgação da obra.

REFERÊNCIA

MIRANDA, Antonio Carlos de Oliveira et al. Modeling 2D surface to 1D through-crack transitions using 2D point load weight function. In: INTERNATIONAL CONFERENCE ON CRACK PATHS, 6., 2018, Verona, Italy.

Modeling 2D Surface to 1D Through-Crack Transitions Using 2D Point Load Weight Function

Antonio Carlos de Oliveira Miranda, Marcelo Avelar Antunes

University of Brasília

acmiranda@unb.br, <https://orcid.org/0000-0002-5225-7428>

marcelo.avelar.antunes@gmail.com, <https://orcid.org/0000-0003-0247-9812>

Marco Antonio Meggiolaro, Jaime Tupiassú Pinho de Castro

Pontifical Catholic University of Rio de Janeiro

meggi@puc-rio.br,

jtcastro@puc-rio.br

ABSTRACT Part-through surface or corner 2D cracks are commonly found in structural components. To model them assuming that the shape of their fronts is approximately elliptic is a quite reasonable hypothesis supported by fractographic observations, but their transition to a 1D through-crack normally is not properly addressed in fatigue life predictions. Although experimental data reveal that the frontier of 2D superficial cracks essentially retain their elliptical shape as they gradually grow into a through-crack, it is usual to assume they are immediately transformed into a 1D through-crack when their depth reaches the cracked component thickness. This oversimplified approximation may create a large jump in stress intensity values, leading to excessively conservative fatigue crack growth predictions, or else the crude shape jump hypothesis may induce false overload events that can much affect fatigue crack growth retardation models, leading to inadmissible non-conservative life predictions. To minimize such problems, a crack propagation strategy, based on a point load weight function, is proposed and verified by 2D crack propagation tests in two different materials, 4340 steel and polycarbonate (PC).

KEYWORDS. Fatigue, Point Load Weight Function, Crack.

INTRODUCTION

Fatigue cracks regularly nucleate as part-through surface or corner cracks that initially grow in two dimensions, and a large part of their fatigue lives can be expended to propagate these relatively short cracks. Whilst growing, these 2D cracks retain an approximately elliptical shape [1], but they can have their aspect ratio a/c changed from cycle to cycle, where a and c are the ellipsis semi-axes. This occurs because their stress intensity factors (SIF) in general vary from point to point along their fronts.

Some analytical expressions are available to quantify the SIFs of elliptical 2D cracks under combined tension and bending [2-3], but the modeling of part-through cracks is still not well developed. The transition behavior of a surface flaw into a through-crack is usually not accounted for when modelling them. It is usually assumed that when submitted to tension loads, the surface crack is immediately transformed into a through-crack when its depth a reaches the thickness of the specimen t at the back surface of the cracked component. Based on an ill-defined “catch up effect” [4], this approximation assumes that the crack front at the back-surface experiences a much higher SIF than at the front surface, which would almost instantaneously straighten the profile of the crack, transforming it into an 1D crack. Besides being too simplistic, this approach creates a discontinuity in the computed SIF, often providing excessively conservative crack growth predictions.

POINT-LOAD WEIGHT FUNCTION IMPLEMENTATION

Jankowiak et al. [5] demonstrated that SIF calculations and fatigue crack growth analyses of cracks with irregular front shapes can be much improved with the use of suitable point-load weight functions (WF). The

first step in this modeling approach consists in approximating the crack frontiers by rectilinear segments (Fig.1), and then computing its inverted boundary, Γ_C , as the sum of all inverted contours, Γ_{Ci} , corresponding to each linear segment of the crack frontiers:

$$\Gamma_C = \sum_{i=1}^n C_i \quad (1)$$

where

$$\Gamma_{Ci} = \frac{1}{2 S_{\rho i}} \Delta \alpha_i \quad (2)$$

In the case of embedded cracks in finite bodies, not only the shape of their fronts, but also their external boundary effects must be properly considered when calculating the SIF distribution along the crack front. To do so, Glinka and Reinhardt [6] proposed a weight function that can be used for the purposes of the present work as well:

$$m_a(x, y) = \frac{\sqrt{2}}{\pi \rho^2} \frac{\sqrt{\Gamma_C + \Gamma_B}}{\Gamma_C} \quad (3)$$

where the arc length, Γ_B , represents the length of the external boundary contour.

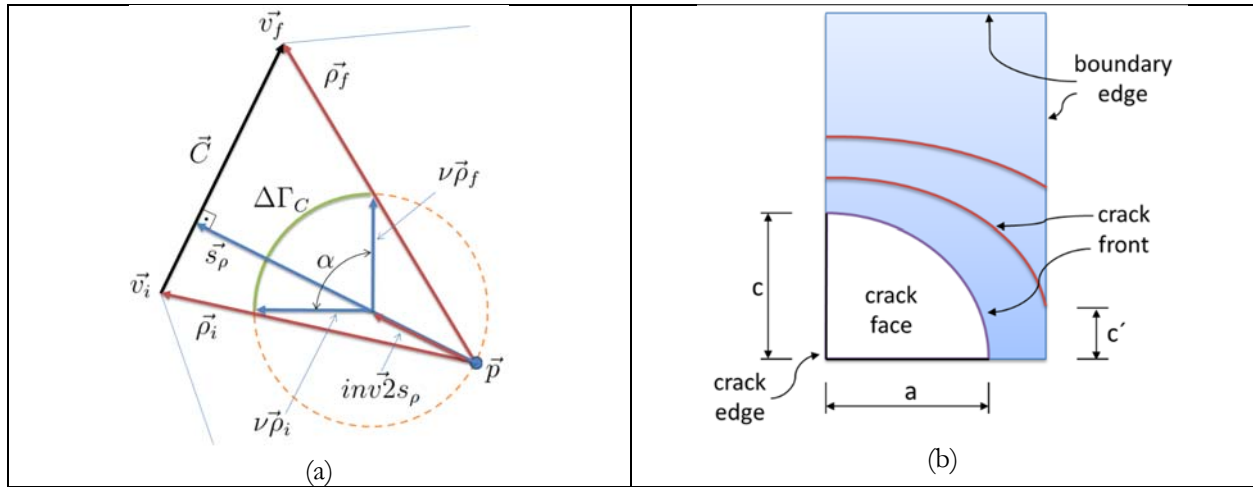


Figure 1- (a) Inverted boundary definitions; (b) crack front, crack front, crack edge, crack face and dimensions definitions.

This numerical approach has been implemented in this work using the relatively simple algorithm depicted in Figure 2. Once the inverted boundary is quantified, the calculation of the SIF for any point along the crack front requires the summation of all products of the point-load weight function, $m(x,y)$, by the loads $F(x,y)$, resulting from the stress field, $\sigma(x,y)$, acting over all crack surface area elements, $dx dy$:

$$K_A = \sum_{j=1}^l F_j(x, y) m(x_j, y_j) \quad (4)$$

where

$$F_j(x, y) = \int_{x_j-dx/2}^{x_j+dx/2} \int_{y_j-dy/2}^{y_j+dy/2} \sigma(x, y) dx dy \quad (5)$$

The algorithm used to compute the SIF distribution along the crack front is depicted in Figure 3.

Algorithm 1: Inverted boundary

Data: L , List with all segments of a boundary \vec{p} , reference point to compute inverted boundary**Result:** Γ_C inverted boundary

```
1  $\Gamma_C \leftarrow 0$ 
2 foreach segment  $s_i$  in  $L$  do
3    $\vec{v}_i \leftarrow$  get initial vertex of segment  $s_i$ 
4    $\vec{v}_f \leftarrow$  get final vertex of the segment  $s_i$ 
5    $\vec{C} \leftarrow \vec{v}_f - \vec{v}_i$ 
6    $\vec{\rho}_i \leftarrow \vec{v}_i - \vec{p}$ 
7    $\vec{\rho}_f \leftarrow \vec{v}_f - \vec{p}$ 
8    $\vec{N} \leftarrow \begin{Bmatrix} -C_y \\ C_x \end{Bmatrix}$ 
9    $\vec{n} \leftarrow \vec{N} / \|\vec{N}\|$ 
10   $d \leftarrow \vec{\rho}_i \cdot \vec{n}$ 
11   $\vec{s}_\rho \leftarrow \vec{n} \cdot d$ 
12   $inv2s_\rho \leftarrow \vec{s}_\rho \cdot 0.5 / (\vec{s}_\rho \cdot \vec{s}_\rho)$ 
13   $inv\rho_i \leftarrow \vec{\rho}_i / (\vec{\rho}_i \cdot \vec{\rho}_i)$ 
14   $inv\rho_f \leftarrow \vec{\rho}_f / (\vec{\rho}_f \cdot \vec{\rho}_f)$ 
15   $\nu\vec{\rho}_i \leftarrow inv\rho_i - inv2s_\rho$ 
16   $\nu\vec{\rho}_f \leftarrow inv\rho_f - inv2s_\rho$ 
17   $\alpha \leftarrow \arccos((\nu\vec{\rho}_i \cdot \nu\vec{\rho}_f) / (\|\nu\vec{\rho}_i\| \cdot \|\nu\vec{\rho}_f\|))$ 
18   $\Delta\Gamma_C \leftarrow \|inv2s_\rho\| \cdot \alpha$ 
19   $\Gamma_C \leftarrow \Gamma_C + \Delta\Gamma_C$ 
20 end
```

Figure 2 – Algorithm to compute inverted boundary.

Algorithm 2: Compute K_I on crack front

Data: L_{CF} , list with all segments of the crack front L_{CE} , list with all segments of the crack edge L_{BE} , list with all segments of the boundary edge M_{BE} , mesh with all triangles on the surface crack**Result:** L_{KI} list of K_I compute on the middle of each segment in the list L_{CF}

```
1 foreach triangle  $t_i$  in the mesh  $M_{BE}$  do
2    $\vec{c}_i \leftarrow$  get center of triangle  $t_i$ 
3    $\Gamma_{Ci} \leftarrow$  Inverted boundary ( $L_{CF}, \vec{c}_i$ )
4    $area \leftarrow$  get area of triangle  $t_i$ 
5    $\sigma \leftarrow$  get stress tension in  $\vec{c}_i$ 
6    $P_i \leftarrow area \cdot \sigma$ , result force in the center of triangle  $t_i$ 
7 end
8 foreach segment  $s_j$  in the list  $L_{CF}$  do
9    $\vec{c}_s \leftarrow$  get center of segment  $s_j$ 
10   $\Gamma_{CE} \leftarrow$  Inverted boundary ( $L_{CE}, \vec{c}_s$ )
11   $\Gamma_{BE} \leftarrow$  Inverted boundary ( $L_{BE}, \vec{c}_s$ )
12   $K_{Ij} \leftarrow 0$ , init  $K_I$  for segment  $s_j$ 
13  foreach triangle  $t_i$  in the mesh  $M_{BE}$  do
14     $\vec{\delta} \leftarrow \vec{c}_i - \vec{c}_s$ 
15     $\rho^2 \leftarrow \vec{\delta} \cdot \vec{\delta}$ 
16     $K_{Ij} \leftarrow K_{Ij} + P_i \cdot \frac{\sqrt{2}}{\pi \cdot \rho^2} \cdot \frac{\sqrt{\Gamma_{Ci} + \Gamma_{CE} + 2.3 \cdot \Gamma_{BE}}}{\Gamma_{Ci}}$ 
17  end
18   $L_{KI} \leftarrow K_{Ij}$ , insert  $K_{Ij}$  in the list  $L_{KI}$ 
19 end
```

Figure 3 – Algorithm to compute SIF on crack front.

EXPERIMENTAL DATA

In order to validate the proposed methodology, the numerical predictions are compared with suitable experimental data obtained from 2D fatigue crack growth (FCG) tests made with two very different materials, polycarbonate (PC) and 4340 steel. PC was selected because it is a transparent and relatively tough polymer, which facilitates the acquisition of crack front images while the fatigue crack propagates. However, since it has long been recognized that its FCG $da/dN \times \Delta K$ behavior is very dependent on hard-to-control environmental parameters [7-12], the PC fatigue tests are considered here qualitatively only, since they could not yield reliable quantitative FCG rate data. Nevertheless, as PC presents a relatively well-defined $da/dN \times \Delta K$ curve under ideal conditions, their tests can also be used to validate the overall predictions of the fatigue analyses presented here.

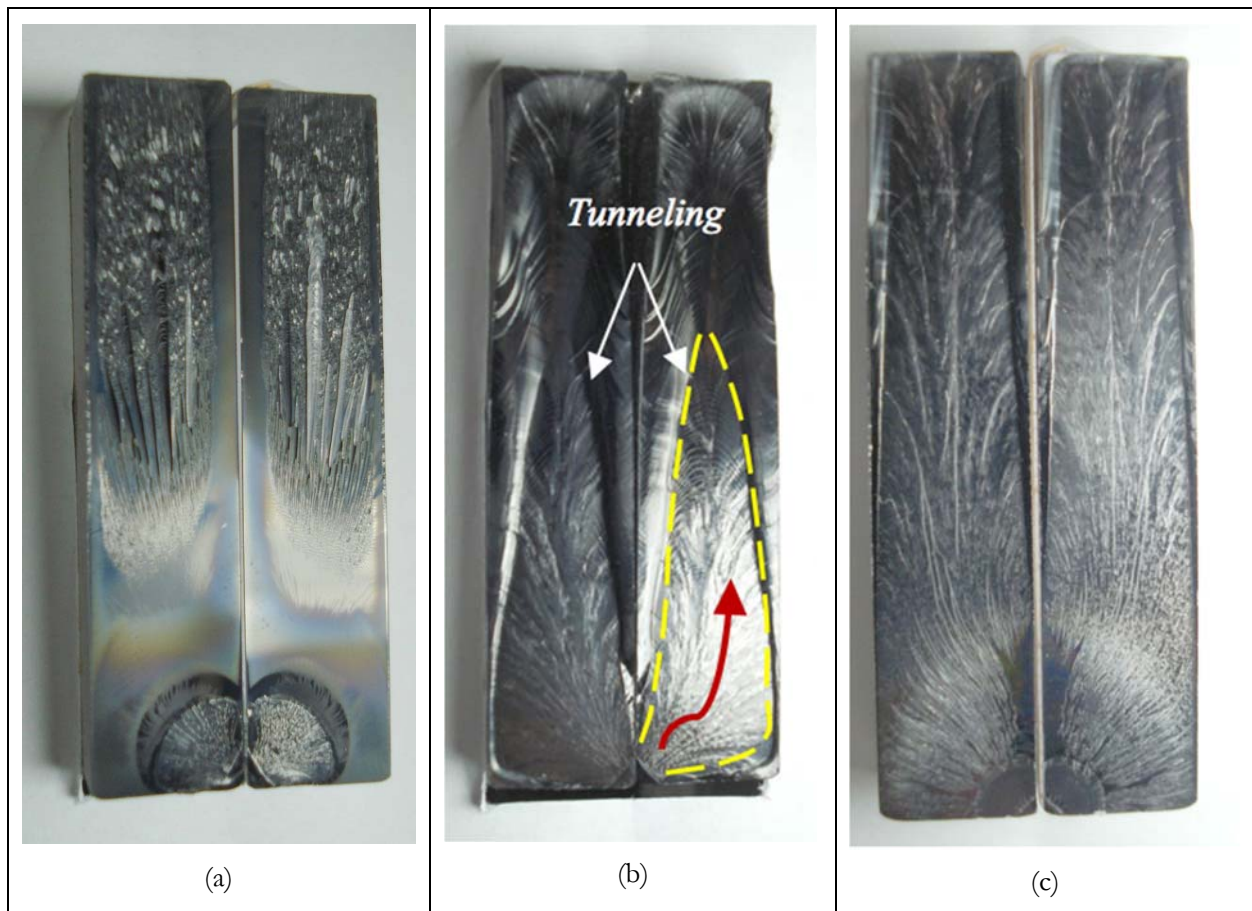


Figure 4 – Experimental results with PC.

Fatigue crack growth (FCG) tests were performed on 365x47x10mm rectangular tension specimens. First, a small initial triangular notch was machined on the corner of each specimen with a size between 1 and 2mm, which was then propagated by fatigue. Two digital cameras and one microscope are used to measure the FCG behavior during the fatigue tests. An $R = 0.1$ load ratio was used for all tests.

The first set of tests was performed under constant amplitude loads. However, the cracks propagated only in their 2D phase with $a/t < 1$, so they did not enter the 2D-1D phase transition, as the PC fracture toughness was reached before that. Indeed, their SIFs increase relatively fast as the cracks grow and, at the same time, despite its relatively high toughness, the SIF range in the $da/dN \times \Delta K$ PC curve is still very narrow (between 0.5-5MPa \sqrt{m}). Figure 4(a) show an example of these results.

To avoid this undesired behavior, a second set of PC specimens was tested under decreasing load ranges. However, even this precaution was not enough to eliminate the experimental problems. As a matter of fact, although their cracks did reach the transition from 2D to 1D, high plasticity occurred on these specimen surfaces, creating significant tunneling effects [12,13], as shown in Figure 4(b).

Therefore, a third set of PC tests was performed to properly simulate the desired 2D-1D crack transition, maintaining the SIF ranges low and approximately constant, $\Delta K_I(a) = \Delta K_I(c) \cong 1\text{MPa}\sqrt{\text{m}}$, gradually reducing the applied load on the PC specimens as the crack propagated to obtain the desired well behaved 2D-1D transition. Well-defined beach marks were finally obtained with this procedure, and helped to track the crack front lines as the crack grew by fatigue, as shown in Figure 4(c).

As previously stated, because of the experimental problems faced in reproducing smooth 2D-1D crack transitions in the PC specimens, additional FCG tests were performed on similar 200×21.5×10mm rectangular specimens made of annealed SAE 4340 steel. Initial triangular notches were also machined on the corner of these specimens, with an initial size ranging from 2 to 3 mm. A microscope was used to obtain the crack positions on different faces of the specimens, measuring them from digital images. The fatigue tests were performed at frequencies between 10 and 20Hz in a 100kN computer-controlled servo-hydraulic testing machine, with a baseline SIF range between $\Delta K_I \cong 20\text{MPa}\sqrt{\text{m}}$ and $\Delta K_I \cong 60\text{MPa}\sqrt{\text{m}}$, both with $R = 0.1$. The annealed SAE 4340 tested steel has yield strength $S_Y = 377\text{MPa}$, ultimate strength $S_U = 660\text{MPa}$, Young's modulus $E = 205\text{GPa}$, and reduction in area $RA = 52.7\%$, measured according to the ASTM E 8M-99 standard, and analyzed weight percent composition 0.37C, 1.53Ni, 0.64Cr, 0.18Mo, 0.56Mn, 0.14Si, 0.04S, 0.035P. Its phase II $da/dN \times \Delta K$ data, obtained under a stress ratio $R = 0.1$ and measured following ASTM E 647-99 procedures, can be fitted by a Paris equation $da/dN = 2.5 \cdot 10^{-9} \cdot \Delta K^{2.48}$ mm/cycle.

Two 4340 alloy steel specimens were tested, named S10 and S11. To avoid early crack rupture during the desired 2D-1D transition during their FCG tests, the applied load was gradually decreased as the cracks grew to maintain a quasi-constant SIF range $\Delta K \cong 24\text{MPa}\sqrt{\text{m}}$.

Figure 5(a) shows the fracture surface of the S10 specimen, depicting its fatigue crack with several crack fronts enhanced to display their shapes along the 2D-1D transition. This figure clearly demonstrates how simplistic the still usual “instantaneous” 2D-1D transition hypothesis is for FCG simulations. Figure 5(b) shows the normalized SIF along several crack fronts. The first curve (black) is the crack front before the transition. It is possible to note an increased in the SIF along the crack fronts, obtained by the point-load weight function approach, on right side face of specimen. It is this SIF variation along the crack fronts that drives the gradual 2D-1D transition, forcing the right side of the subsequent crack fronts to catch up their left size.

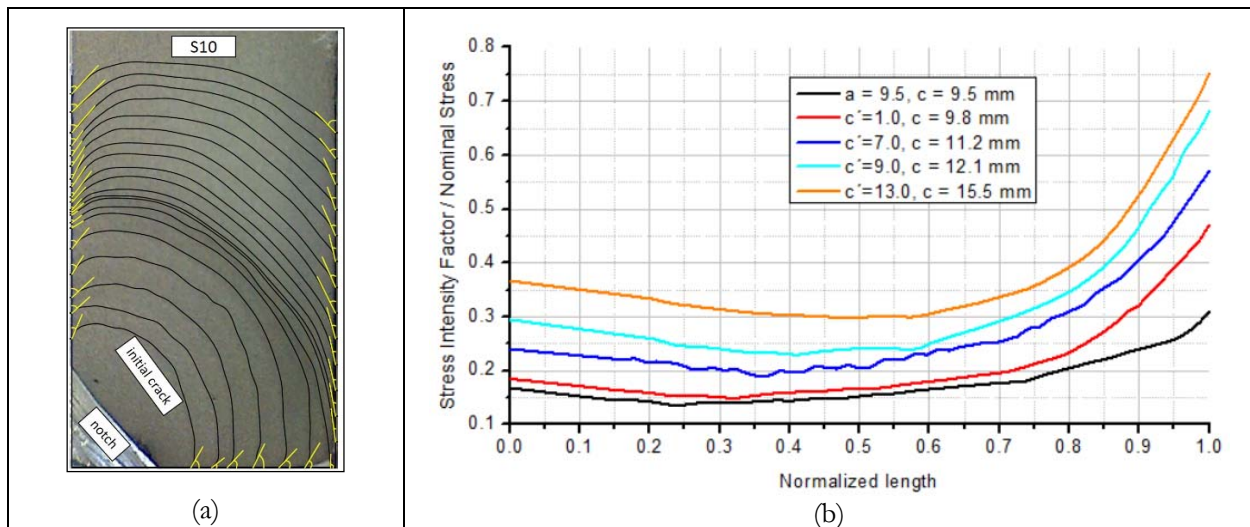


Figure 5 – (a) Experimental crack propagation S10; (b) SIF on crack front computed by point load weight function.

CONCLUSION

This work presented a detailed implementation of a simple numerical approach based on point-load weight functions to compute SIFs of complex crack fronts along 2D to 1D transitions during FCG tests. The implementation is based on a definition of an inverted boundary, for which an algorithm is proposed. A cross section of a cracked specimen is defined by the crack front, the crack edges and the boundary edges. The crack surface is approximated by a set of triangles. Another algorithm was present to compute the SIFs along the crack fronts. To validate and understand the proposed methodology, experimental data obtained on suitable FCG tests of two very different materials, polycarbonate (PC) and 4340 steel, is presented and analyzed. PC was selected because it is a transparent and relatively tough polymer, thus facilitating the acquisition of crack front images whilst the fatigue crack propagates. Two 4340 alloy steel specimens were tested, applying the load gradually to maintain a quasi-constant SIF. With the obtained experimental crack fronts, it is possible to numerically compute the SIF distribution along their crack fronts during the 2D to 1D transitions.

ACKNOWLEDGMENT

This work has been supported by University of Brasília and FAPDF - Foundation for Research Support of the Federal District.

REFERENCES

- [1] Castro,JTP; Giassoni,A; Kenedi,PP. Fatigue propagation of semi and quart-elliptical cracks in wet welds. *J Brazilian Soc Mech Sci Eng* 20:263-277, 1998.
- [2] T. L. Anderson, *Fracture Mechanics: Fundamentals and Applications*, 2nd ed. Taylor & Francis, 1994.
- [3] Castro,JTP; Meggiolaro,MA. *Fatigue Design Techniques*, volume 3: Crack Propagation, Temperature and Statistical Effects. CreateSpace 2016.
- [4] Grandt,AF; Harter,JA; Heath;BJ. Transition of part-through cracks at holes into through-the-thickness flaws. *ASTM STP* 833:7-23, 1994.
- [5] Jankowiak,A; Jakubczak,H; Glinka,G. Fatigue crack growth analysis using 2-D weight function. *Int J Fatigue* 31:1921-1927, 2009.
- [6] Glinka,G; Reinhardt;W. Calculation of stress intensity factors for cracks of complex geometry and subjected to arbitrary nonlinear stress fields. *ASTM Fatigue and Fracture Mechanics: 31st Volume*, 2000.
- [7] Hertzberg,RW; Nordberg,H; Manson;JA. Fatigue crack propagation in polymeric materials. *J Mater Sci* 5:521-526, 1970.
- [8] Kitagawa,M. Fatigue crack growth in polycarbonate. *Bulletin JSME* 17:427-433, 1974.
- [9] Martin,GC; Gerberich;WW. Temperature effects on fatigue crack growth in polycarbonate. *J Mater Sci* 11:231-238, 1976.
- [10] Radon,JC; Chauhan,P; Culver;LE. The influence of temperature and frequency on fatigue crack propagation in polymers. *Colloid Polymer Sci* 254:382-388, 1976.
- [11] Fraser;RAW; Ward;IM. Temperature dependence of craze shape and fracture in polycarbonate. *Polymer* 19:220-224, 1978.
- [12] Sehanobish,K; Haddaoui,N; Moet;A. Effect of thickness on ductile fatigue crack propagation in polycarbonate. *J Mater Sci* 28:1360-1366, 1993.
- [13] Zuo,J; Deng,X; Sutton;MA. Crack tunneling: effect of stress constraint. *ASME 2004 Int Mech Eng Cong Exposition*, Anaheim, California, USA, 2004.